Nanoscale

PAPER

View Article Online
View Journal | View Issue

Cite this: *Nanoscale*, 2026, **18**, 1433

Size effects in magnetic separation for rapid and efficient bacteria removal

Jingge Chen,[a,b] Alicia M. Chandler,[b] Indrek Külaots,[b] Qingbo Zhang[c] and Vicki L. Colvin *[a,b,c]

Magnetic separation offers a promising strategy for bacterial removal from aqueous systems due to its tunable specificity, biocompatibility, and facile recovery. However, the influence of nanoparticle size on removal efficiency and adsorption capacity remains unclear. Here, we systematically investigate size-dependent effects using porous magnetic particles covalently modified with polyethyleneimine (PEI). Porous magnets with diameters ranging from ~50 to ~420 nm were synthesized and functionalized with PEI to enhance electrostatic interactions with negatively charged bacteria. The resulting PEI-modified porous magnets induced extensive bacterial aggregation and exhibited high adsorption capacities for both Gram-negative *Escherichia coli* and Gram-positive *Staphylococcus aureus*. Adsorption capacity increased with decreasing particle size under equal iron mass, reaching up to 18.8×10^9 CFU mg^{-1} for *E. coli* and 28.9×10^9 CFU mg^{-1} for *S. aureus*. Adsorption kinetics were also size-dependent, reaching over 95% of maximum capacity within 10 minutes for all particle sizes. The smallest particles (50 nm) were difficult to recover without sufficient bacterial contact. In low-concentration bacterial separations, larger particles resulted in minimal residual bacteria and achieved nearly 100% removal. These results highlight the critical role of particle size in magnetic bacterial separation and provide guidance for designing efficient magnetic adsorbents.

Received 1st September 2025,
Accepted 30th November 2025

DOI: 10.1039/d5nr03699b

rsc.li/nanoscale

1. Introduction

Bacterial contamination remains a leading cause of human disease.[1] In recent years, bacterial contamination has become increasingly severe due to the rise of antibiotic resistance and the formation of biofilms.[2–4] Rapid and efficient bacterial separation is essential for applications including water treatment, food safety, disease diagnosis, and therapeutic interventions.[5–8] Additionally, emerging synthetic biology approaches increasingly rely on the handling of large populations of genetically engineered bacteria.[9,10] This growing industry further amplifies the demand for effective bacterial separation techniques.[11] Conventional methods such as centrifugation, filtration, electrophoresis, and flocculation often suffer from low specificity, limited efficiency, or secondary contamination, highlighting the need for alternative strategies.[12] In contrast, magnetic separation holds great promise due to its tunable specificity, remote controllability, high biocompatibility, and efficient recoverability.[13]

In the past decades, magnetic bacteria separation has made considerable progress and emerged as one of the most versatile strategies for various biomedical and environmental applications.[14] Many magnetic nanoparticles are surface-functionalized to target specific bacteria, enabling their separation using external magnetic fields.[15] Common surface coatings include polymers, inorganic composites, and biological molecules, which interact with bacteria *via* electrostatic forces, hydrogen bonding, or specific biological recognition.[16–18] In addition to magnetic separation, these functional magnetic materials can also facilitate bacterial detection *via* colorimetric, fluorescent, and surface-enhanced Raman signals, leveraging their physicochemical properties.[19–22] Magnetic nanoparticles can further enable bacterial imaging, exert antibacterial effects, and disrupt biofilms through techniques such as magnetic resonance imaging, magnetic drug delivery, magnetic hyperthermia, and magnetic robotic actuation, offering valuable tools for bacterial diagnosis and treatment.[2,23,24] Despite these advances, many studies focus on proof-of-concept demonstrations and face challenges such as low separation efficiency, high cost, and limited scalability. The need for improved separation performance has motivated researchers to enhance magnetic adsorbents and systematically investigate how their physicochemical properties influence bacterial removal.

[a]*Institute for Biology, Engineering, and Medicine, Brown University, RI 02912, USA. E-mail: vicki_colvin@brown.edu*
[b]*School of Engineering, Brown University, RI 02912, USA*
[c]*Department of Chemistry, Brown University, Providence, RI 02912, USA*

Particle size is a critical factor affecting the performance of magnetic separation.[25] On one hand, particle size strongly influences the motion of magnetic nanoparticles within their surrounding medium.[26] As the size of magnetic nanoparticles increases, their magnetic moment, and the magnetic force they experience also increase, which can substantially reduce the separation time by several orders of magnitude.[8,27] On the other hand, smaller magnetic particles possess larger specific surface areas and exhibit more intense Brownian motion, which can enhance their attachment to bacteria.[28] However, the interplay between these factors complicates the prediction of size-dependent effects on bacterial separation.[29,30]

Here, we investigate the size effects of porous magnetic particles on bacterial separation. Porous magnets, also referred to as magnetic clusters, are chosen as the magnetism provider. Compared with other magnetic materials, an extraordinarily wide size range (~50–420 nm) could be achieved through our modified synthesis strategy, enabling systematic exploration of size-dependent effects. Moreover, their porous structure disrupts the anisotropy of magnetic crystals, allowing the particles to maintain minimal coercivity even at hundreds of nanometers in size, thereby preventing aggregation caused by remanent magnetism. Polyethyleneimine (PEI), a highly cationic polymer with a dense array of amino groups, was covalently grafted onto the porous magnets to promote electrostatic attachment to negatively charged bacteria. PEI modification was achieved either *via* (3-aminopropyl)triethoxysilane (APTES) and glutaraldehyde as cross-linking agents or through EDC/NHS chemistry. Representative bacteria, *Escherichia coli* (*E. coli*) and Gram-positive *Staphylococcus aureus* (*S. aureus*), were selected as targets because they are common biological contaminants responsible for various infectious diseases.[15] Both low- and high-concentration bacterial separation experiments were conducted to evaluate adsorption capacity, removal efficiency, and separation kinetics, allowing a comprehensive assessment of particle size effects.

2. Materials and methods

2.1. Chemicals and materials

Ethylene glycol (anhydrous, 99.8%), iron(III) chloride hexahydrate ($FeCl_3{\cdot}6H_2O$, ACS reagent, 97%), urea (ACS reagent, 99.0%), acetone (ACS reagent, ≥99.5%), methanol (suitable for HPLC, ≥99.9%), toluene (anhydrous, 99.8%), iron standard solution ($Fe(NO_3)_3$ in HNO_3 0.5 mol L^{-1} 1000 mg L^{-1} Fe Certipur®), nitric acid (HNO_3, ACS reagent, 70%), polyethylenimine (PEI, branched, average $M_w \sim 25\,000$ Da), glutaraldehyde solution (50 wt% in H_2O), (3-aminopropyl)triethoxysilane (APTES, 99%), 2-(*N*-morpholino)ethanesulfonic acid (MES, 99%) were purchased from Sigma-Aldrich. Polyacrylic acid sodium salt (PAA, $M_w \sim 6000$ Da) was from Polyscience Inc. 1-Ethyl-3-(3-dimethylaminopropyl)carbodiimide hydrochloride (EDC), sulfuric acid (ACS grade, 98%), hydrochloric acid (ACS grade, 37%) and hydrogen peroxide (30%) were purchased from Fisher Scientific. The UranyLess electron microscope stain was purchased from Electron Microscopy Science (Hatfield, PA). *E. coli* strain MG1655 (CGSC# 6300) was obtained from the Coli Genetic Stock Center (Keio Collection, Yale University). *S. aureus* strain (ATCC# 25923) was provided by Prof. Anita Shukla from Brown University.

2.2. Preparation of porous magnets

Porous magnets with different dimensions were synthesized according to a well-developed hydrothermal method (also referred to as the "polyol" synthesis) with specific modification. Prior to experiments, PAA was dissolved in ultrapure water to prepare uniform solutions (50 and 100 μg μL^{-1}). In each reaction, 540 mg of $FeCl_3{\cdot}6H_2O$, 1200 mg of urea and different volumes of premade PAA solutions were dissolved in 20 mL of ethylene glycol under mechanical stirring (600 rpm, 30 min). The dosage of PAA solutions used in different reactions were 2000P100 (2000 μL, 100 μg μL^{-1}), 1000P100 (1000 μL, 100 μg μL^{-1}), 500P50 (500 μL, 50 μg μL^{-1}), 300P50 (300 μL, 50 μg μL^{-1}) and 150P50 (150 μL, 50 μg μL^{-1}), respectively. Then, the mixture was transferred into a Teflon-lined stainless steel autoclave reactor (50 mL) and heated under 200 °C for 6 h. After cooling to room temperature, the resultant products were washed with acetone and ultrapure water several times through magnetic separation. The synthesized products were redispersed in ultrapure water for surface modification.

2.3. Surface modification of porous magnets

Prior to surface modification experiments, PEI was dissolved in ultrapure water to prepare a uniform solution in a 60 degrees Celsius water bath. Four sizes of porous magnets synthesized with PAA dosages of 150P50, 300P50, 500P50 and 1000P100 were functionalized with PEI with APTES and glutaraldehyde as cross-linkers. In detail, premade particles were washed with methanol several times to remove water inside and then dissolved in 200 mL of 50/50 (v/v) methanol/toluene mixture solution, which were added 2 mL of APTES and kept stirring overnight.[31] Following on, APTES modified porous magnets were washed several times with water and dissolved in 800 mL of ultrapure water together with 1 mL of PEI solution (100 mg mL^{-1}). Then, 100 mL of diluted glutaraldehyde solution (0.001%) was added dropwise, and the mixed solution was kept stirring for 2 h.

Another size of porous magnet synthesized with PAA dosages of 2000P100 was modified with PEI through EDC/NHS chemistry. In detail, premade particles were diluted with 800 mL of ultrapure water and stirred in a 2000 round-bottom flask. Then, 50 mg EDC, 100 mg MES and 1 mL of PEI solution (100 mg mL^{-1}) were added into the flask and the mixture was kept stirring for 2 h (1000 rpm). The resultant products were washed with ultrapure water several times through magnetic separation. The concentration of PEI modified porous magnet solutions was determined by inductively coupled plasma emission spectrometry (ICP-OES, iCAP™ 7400, Thermo Fisher Scientific) upon digestion with nitric acid and hydrogen peroxide.

2.4. Materials characterization

The morphology of porous magnets was characterized by transmission electron microscopy (TEM) through a JEOL 2100 Field Emission Gun Transmission Electron Microscope machine at an acceleration voltage of 200 kV. A drop of porous magnet solution with a concentration of 100–300 ppm was dropped on a 200-mesh carbon-coated copper grid and let stand at room temperature overnight to allow the complete evaporation of water. The particle size was analyzed by ImageJ and over a hundred particles were recorded to report average size as well as size distribution.

The crystal structure of porous magnets was obtained by X-ray diffractometry (XRD) with a Bruker D8 20 Discovery 2D X-ray Diffractometer (Cu Kα, λ = 1.54056 Å). 10 to 50 mg of dried sample was placed on a microscope slide and pressed even by a cover slide. The full width at half maximum (FWHM) of the (311) peak centered at 35.4° was measured using Origin peak analysis function. The grain size of each sample was calculated based on Debye Scherrer equation: grain size = λ/FWHM cos(θ).

The magnetic properties of porous magnets were evaluated by the vibrating-sample magnetometer (VSM, Lake Shore 7400 Series VSM). Approximately 10 mg of sample was placed in a powder sample holder for measurements. The hysteresis loop was recorded from 10 000 to −10 000 oersted (Oe) at room temperature.

The sample's Specific Surface Area (SSA) and porosity were determined using an Anton-Paar (formerly Quantachrome) Autosorb-1 instrument. In these experiments, approximately 50 to 100 mg of sample was outgassed at 250 °C for 24 h. The N_2 adsorption–desorption isotherms were obtained by recording data points at relative pressures (P/P_0) from 10^{-6} to 1 at a temperature of 77 K. The SSA values were calculated by applying the Brunauer–Emmett–Teller (BET) model and the pore size distributions using the non-local density functional theory (NLDFT) slit pore model.[32] Micropore volume and micropore SSA were also determined by applying the Dubinin–Radushkevitch (DR) theory.

The functional groups of PEI modified porous magnets were analyzed by Fourier transform infrared spectroscopy (FTIR) using a IRAffinity-1S FTIR Spectrometer (Shimadzu). Approximately 10 mg of sample was placed on the center of detection area. The spectra were collected from 4000 to 400 cm^{-1} at room temperature.

The hydrodynamic size distribution and Zeta potential of porous magnets before and after PEI modification were measured by Zetasizer Nano ZS (Malvern Instruments Ltd). One milliliter of particle solution with a concentration of 100–300 ppm was placed in plastic cuvettes designed for size and zeta potential measurements. The particle solution was equilibrated for 2 minutes at 25 °C before data collection. Each sample was measured three times. The hydrodynamic size was derived from Z average size. The error bar was the standard deviation of three measurements.

The interaction of bacteria and porous magnets was characterized by scanning electron microscopy (SEM, Apreo Volume Scope). A drop of UranyLess contrast stain was reacted with bacteria samples on copper grids for 50 seconds to improve imaging.

2.5. Bacteria separation

E. coli and *S. aureus* bacteria were grown overnight in 100 mL of Luria–Bertani (LB) broth media at 200 rpm (37 °C). The cell cultures were centrifuged, and the bacteria samples were redispersed in ultrapure water. The concentration of bacteria was determined by serial dilution with subsequent plating on agar plates and measurement of colony forming units (CFUs). When the optical density (OD) at 600 nm of *E. coli* and *S. aureus* bacteria suspensions reached 1.0, their concentrations were ~1.0×10^9 and ~1.5×10^9 CFU mL^{-1}.

All adsorption experiments were performed in culture tubes at 25 ± 2 °C. Normally, PEI modified porous magnets (0.2 mL, 1 mg mL^{-1}) were added into bacteria solutions (2 mL) and incubated for 30 minutes in a shaker (200 rpm). PEI functionalized 2000P100 porous magnets showed extraordinarily high separation capacity and the experiment condition was adjusted to 5 mL of bacteria solution and 0.1 mL of particle solution (1 mg mL^{-1}). In high concentration bacteria separation, the initial OD of bacteria suspension ranged from 0.1 to 0.8. In low concentration bacteria separation, bacteria solution was serially diluted to achieve initial concentrations ranging from 10^2 to 10^7 CFU mL^{-1}. To explore separation kinetics, the incubation time was adjusted to 0.5, 1, 2, 3, 5, 10, 20, 30 minutes, respectively. Following on, a strong NdFeB was then applied to separate the magnetic complex. The concentrations of bacteria in supernatants were determined by a combination of OD600 and plate counting. Bacteria suspensions in the OD600 detection range were detected by OD600 and the results were converted to the concentration of bacteria according to preliminary calibration. Bacteria suspensions below OD600 detection limit were detected by plate counting. Taking the volume change of the reaction solution into consideration, the removal efficiency R and adsorption capacity Q of magnetic composites can be evaluated using the following equations:

$$R = \frac{V_0C_0 - V_eC_e}{V_0C_0} \times 100\%$$

$$Q = \frac{V_0C_0 - V_eC_e}{m}$$

where C_0 (CFU mL^{-1}) and C_e (CFU mL^{-1}) are the initial and post-reaction concentrations of bacteria, V_0 (mL) and V_e (mL) are the initial and post-reaction volumes of the reaction solution, and m (g) is the mass of the magnetic composites. Each experiment was repeated three times. The experimental results were averaged, and the standard deviation was taken.

3. Results and discussion

3.1. Preparation and characterization of PEI modified porous magnets

Porous magnets, also known as magnetic clusters, were synthesized using a classical polyol method, in which forced hydrolysis of iron salts generates condensed iron oxide phases that gradually ripen into multicore particles under the influence of surface ligands.[33,34] This process involves complex crystal nucleation, growth, and aggregation steps, and the final particle dimensions are highly sensitive to parameters such as reaction time and temperature, precursor type and concentration, and pretreatment conditions.[35,36] These conditions could be varied to tune the dimensions of the porous magnets.[37,38]

Here, we highlight a synthesis strategy in which the surface ligand and water content in the reaction mixture are deliberately adjusted to control cluster diameter across an exceptionally wide range, enabling a systematic investigation of size effects in magnetic separation for efficient bacterial removal. As illustrated in Fig. 1a, the surface ligand PAA was first dissolved in water, while the remaining reactants were dissolved separately in ethylene glycol before being combined and heated in a sealed autoclave to form porous magnets. This operation enabled product reproducibility as the poor solubility of PAA in ethylene glycol might cause heterogeneous synthesis.[39] At the same time, excellent size control was achieved because crystal growth and aggregation depended critically on the relative amounts of PAA and water in the reaction mixture.[40,41]

As shown in Fig. 1b–f, increasing the amount of PAA solution resulted in progressively smaller particle diameters. Additional TEM images (Fig. S1) confirm that the particles were composed of numerous small primary crystals. The reduction in particle size is likely due to the ability of both PAA and water to suppress crystal aggregation during growth.[37,42] Measured using ImageJ, the average particle diameters were $(4.2 \pm 0.8) \times 10^2$ nm, $(3.6 \pm 0.9) \times 10^2$ nm, $(2.1 \pm 0.5) \times 10^2$ nm, 87 ± 22 nm, and 51 ± 6 nm, respectively. This broad and well-controlled size range provides a robust platform for investigating size-dependent effects in magnetic bacterial separation.[35] For convenience, these porous magnets (PM) were labeled according to their approximate diameters in the following manuscript, which were PM_420 nm, PM_360 nm, PM_210 nm, PM_90 nm, and PM_50 nm.

The X-ray diffractometry (XRD) patterns of these particles in Fig. 2(a) showed strong diffraction peaks at 2θ = 30.1°, 35.4°, 43.3°, 53.6°, 57.0° and 62.7°, which matched well with standard Fe_3O_4 (powder diffraction file card JCPDS No. 19-0629) and corresponded to the (220), (311), (400), (422), (511) and (440) crystal planes.[43,44] According to the Scherrer formula, the crystal sizes of PM_420 nm, PM_360 nm, PM_210 nm, PM_90 nm, and PM_50 nm were calculated as 15.4, 17.9, 18.1, 15.6 and 13.2 nm, respectively. The stacking of small crystals to form large magnetic particles could meet our desires for large magnetic moments and avoid the influence of

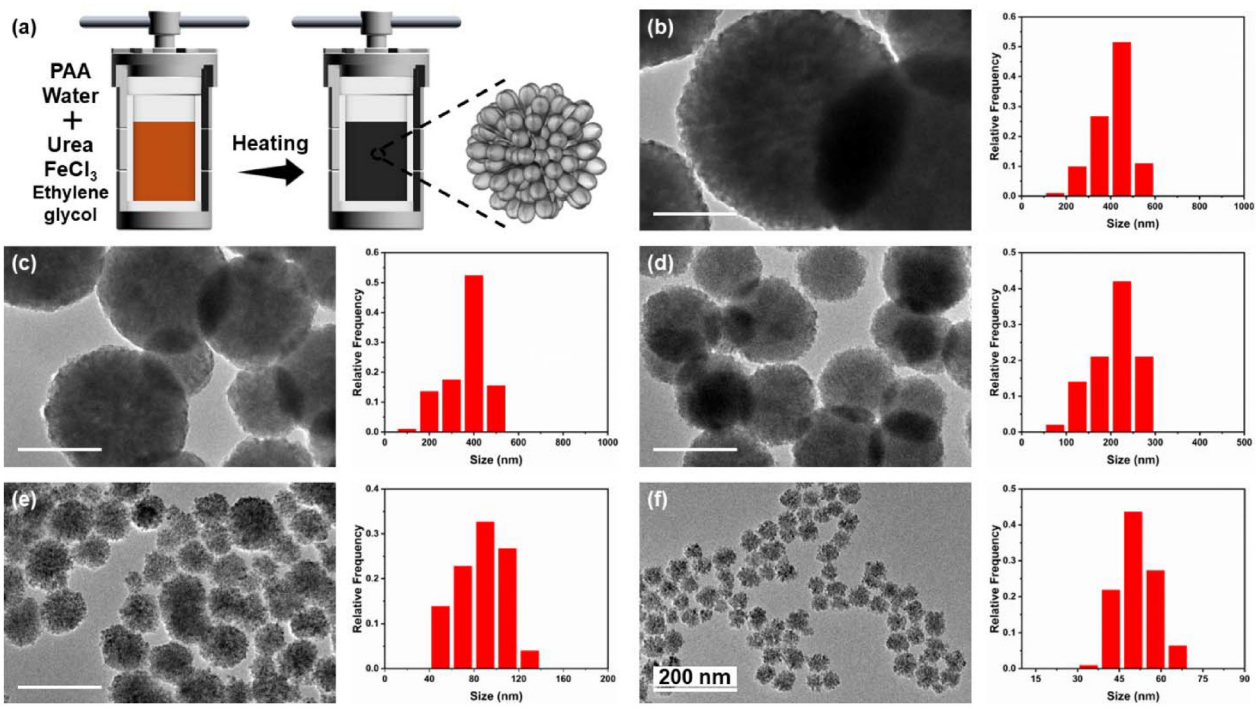

Fig. 1 Preparation and characterization of porous magnets. Synthesis scheme of porous magnets (a). TEM images and size distribution histograms of porous magnets synthesized with different dosages of PAA solution (b: 150 μL, 50 μg μL^{-1}; c: 300 μL, 50 μg μL^{-1}; d: 500 μL, 50 μg μL^{-1}; e: 1000 μL, 100 μg μL^{-1}; f: 2000 μL, 100 μg μL^{-1}). Size distribution histograms summarized over 100 particles in ImageJ.

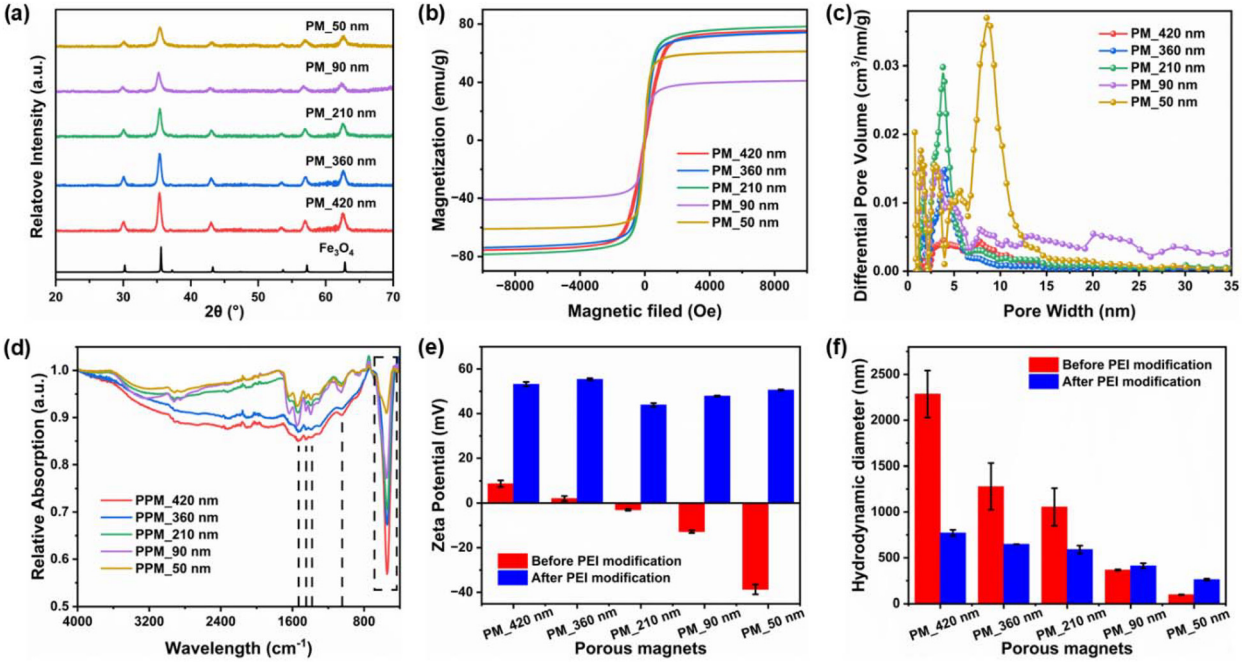

Fig. 2 Characterization of porous magnets before and after PEI modification. The XRD patterns (a), magnetization curves (b) and Non-Local Density Function Theory (NLDFT) slit pore model pore size distribution (c) of porous magnets. The FTIR spectrums of PEI modified porous magnets (d). The zeta potential (e) and hydrodynamic size (f) of porous magnets before and after PEI modification.

anisotropy.[34,45] As shown in Fig. 2(b), all these particles showed almost superparamagnetism even though their diameters were up to hundreds of nanometers. In addition, the saturation magnetization of PM_420 nm, PM_360 nm, PM_210 nm, PM_90 nm, and PM_50 nm were 75.5, 74.0, 78.2, 41.0, 61.0 emu g^{-1}, respectively. The high saturation magnetization and minimum coercivity could ensure quick magnetic response and avoid the influence of particle aggregation caused by coercivity in magnetic separation.[13]

Calculated from nitrogen adsorption–desorption isotherms, the specific surface area (SSA) of PM_420 nm, PM_360 nm, PM_210 nm, PM_90 nm, and PM_50 nm was 19.1, 38.0, 66.5, 79.1, and 114.5 m^2 g^{-1}, respectively. As expected, with the decrease of particle diameters, the SSA increased, which might be because the reduced stacking of small crystals revealed more surface area.[46] Moreover, the pore size distribution of these particles calculated from the non-local density functional theory (NLDFT) slit pore model was shown in Fig. 2(c). Most of these pores or cavities are larger than 2 nm and smaller than 7 nm, *i.e.*, mesopores.[47] Thereinto, particles with approximately 50 nm diameter showed quite a quantity of 10 nm pores, which could be the pores between particles. The calculated total pore volume of PM_420 nm, PM_360 nm, PM_210 nm, PM_90 nm, and PM_50 nm was 0.049, 0.062, 0.118, 0.230, and 0.217 cm^3 g^{-1}, respectively. This suggests that the increase of surface ligands in reactions led to not only smaller particle diameter but also higher pore content, which could be because the size exclusive effect of surface ligands disturbed the compact stacking of small crystals.[48]

PM_420 nm, PM_360 nm, PM_210 nm and PM_90 nm was functionalized with PEI through APTES and glutaraldehyde as cross-linkers, as shown in Fig. S2.[31,49] The concentration of porous magnets and glutaraldehyde in surface modification experiments were adjusted to a very low level to prevent cross linking.[49] Moreover, the smallest PM_50 nm synthesized with substantial PAA as surface ligands was directly reacted with PEI amine groups through EDC/NHS chemistry to enhance surface modification efficiency and further prevent cross linking. PEI modified porous magnets with different diameters were referred to as PPM_420 nm, PPM_360 nm, PPM_210 nm, PPM_90 nm and PPM_50 nm, accordingly.

The Fourier transform infrared spectroscopy (FTIR) spectra of PEI modified porous magnets were shown in Fig. 2(d) and the strong absorption peak at 540 cm^{-1} could be attributed to vibration of Fe–O band at tetrahedral site.[50] The additional absorption peaks at 1044, 1382, 1444, and 1531 cm^{-1} in the FTIR spectra of particles could be attributed to the vibration of C–N, C–C, C–N and N–H bonds, indicating the successful functionalization of PEI.[51–53] TEM images of these particles were shown in Fig. S3, indicating that morphology of these particles was not obviously changed by PEI modification.

Dynamic light scattering (DLS) measurements are shown in Fig. 2e and f. As presented in Fig. 2e, the zeta potentials of PM_420 nm, PM_360 nm, PM_210 nm, PM_90 nm, and PM_50 nm before PEI modification were 8.7 ± 1.5 mV, 2.1 ± 1.1 mV, −3 ± 0.4 mV, −12.8 ± 0.6 mV, and −38.7 ± 2.2 mV, respectively. The slight positive charge of the larger particles likely arises from residual Fe ions on the surface, whereas the

increasingly negative charge of smaller particles is attributed to the higher influence of PAA surfactant.[42] After PEI modification, the zeta potentials increased substantially to 53.2 ± 1 mV, 55.4 ± 0.5 mV, 43.9 ± 0.8 mV, 47.9 ± 0.2 mV, and 50.6 ± 0.2 mV, respectively, confirming successful PEI conjugation. The resulting strong positive surface charge is expected to enhance electrostatic interactions with negatively charged bacterial cells.[54,55] As shown in Fig. 2f, the hydrodynamic diameters of PEI-modified porous magnets also decreased with decreasing particle size, although they remained larger than their corresponding TEM diameters. Therefore, the particles maintained distinct size characteristics sufficient to enable meaningful evaluation of size-dependent effects in subsequent magnetic separation experiments although there might be aggregation or minimal cross-linking between particles.[56]

3.2. Magnetic separation of bacteria

The bacterial separation process using PEI-modified porous magnets is illustrated in Fig. 3(a). After being introduced into bacterial suspensions, the positively charged particles electrostatically interacted with both Gram-negative and Gram-positive bacteria, each of which carries a net negative surface charge.[15] or Gram-negative bacteria, the negative charge primarily originates from lipopolysaccharide (LPS) in the outer membrane, whereas for Gram-positive bacteria it arises from teichoic acids in the cell wall.[57,58] Consistent with these structural features, the measured zeta potentials of the Gram-negative *E. coli* and Gram-positive *S. aureus* strains were −32.6 ± 0.7 mV and −21.8 ± 0.5 mV, respectively. Then, these porous magnets labelled bacteria could be separated by external magnetic fields. The concentrations of bacteria in the supernatant solution were then determined by a combination of OD600 and plate counting. This process is easy to operate, facilitating wide applications.[18]

Besides magnetism driven separation, PEI modified porous magnets could also induce aggregation between bacteria, which could be attributed to charge neutralization and bridging.[59,60] The STEM images of particle/bacteria mixtures

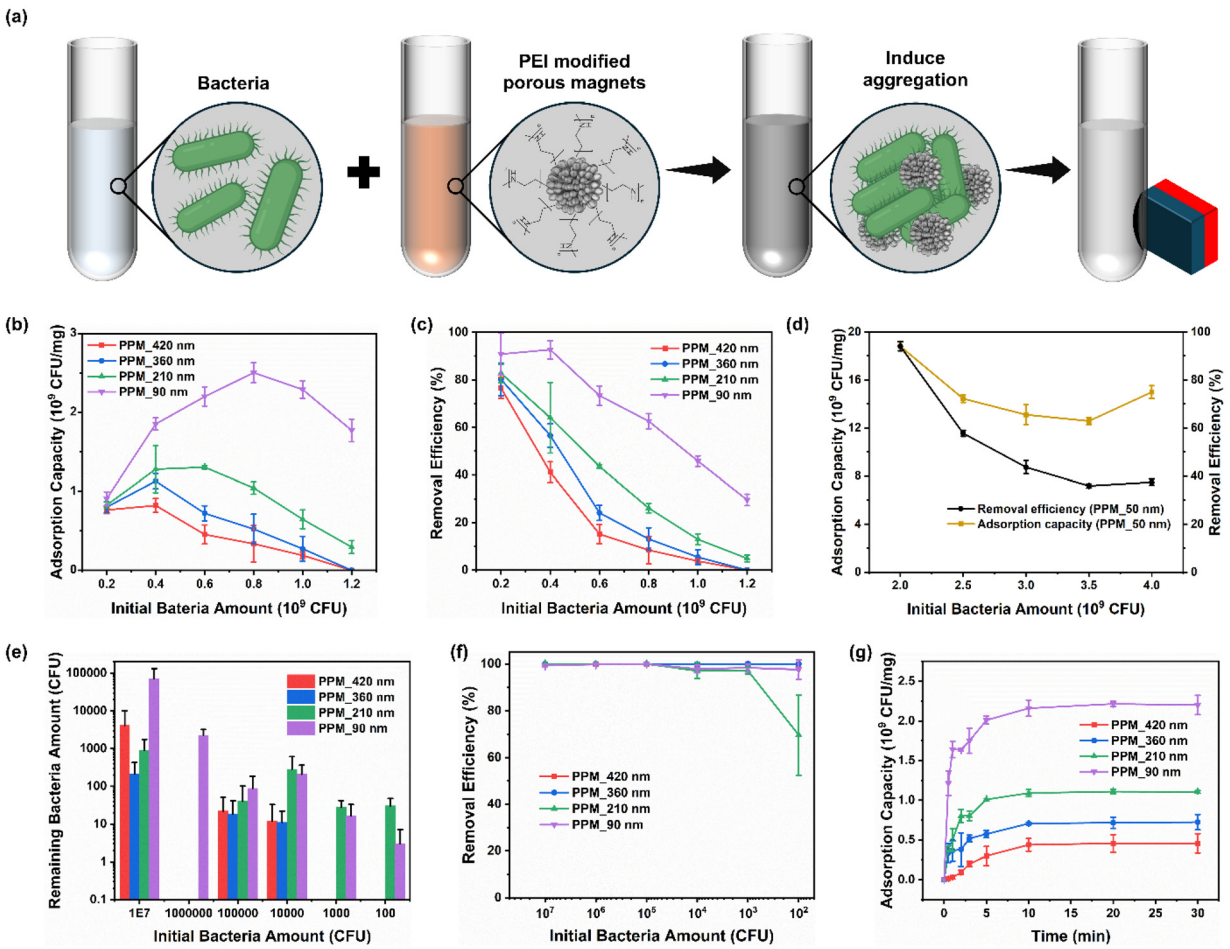

Fig. 3 Magnetic separation of *E. Coli* with PEI modified porous magnets. Scheme of magnetic separation process (a). The adsorption capacity (b) and removal efficiency (c) of PPM_420 nm, PPM_360 nm, PPM_210 nm, PPM_90 nm with different initial bacteria amounts. The adsorption capacity and removal efficiency of PPM_50 nm with different initial bacteria amounts (d). The remaining bacteria amount (e) and removal efficiency (f) of PPM_420 nm, PPM_360 nm, PPM_210 nm, PPM_90 nm in low concentration bacteria separation. The adsorption kinetics of PPM_420 nm, PPM_360 nm, PPM_210 nm, PPM_90 nm (g).

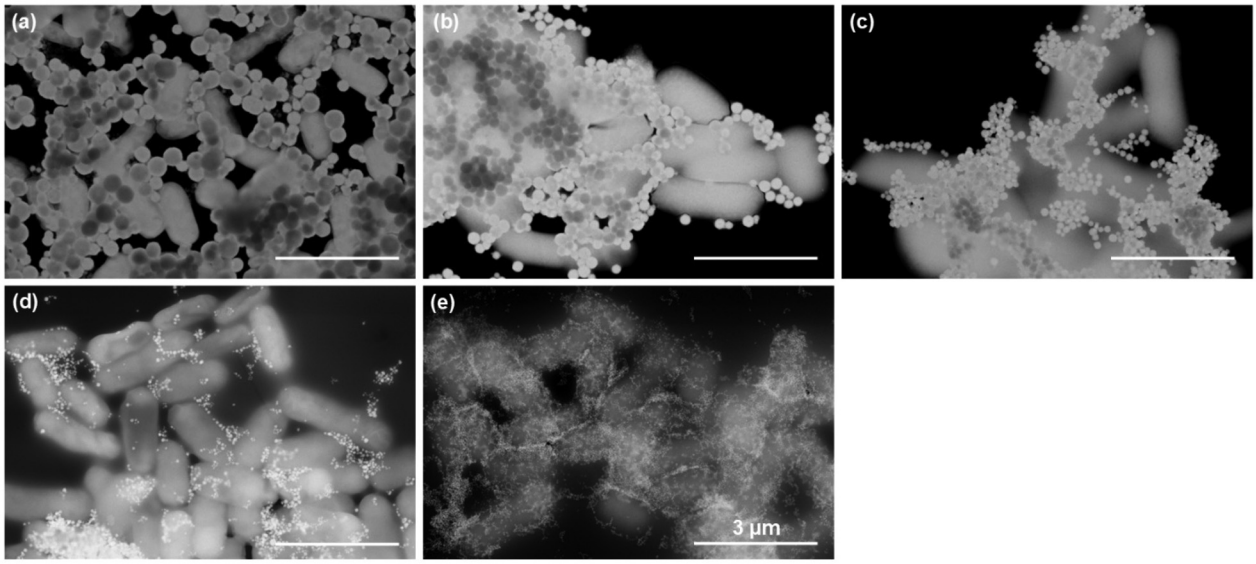

Fig. 4 The STEM images of *E. Coli* interacting with PPM_420 nm (a), PPM_360 nm (b), PPM_210 nm (c), PPM_90 nm (d), and PPM_50 nm (e).

were shown in Fig. 4, exhibiting that particles bridged bacteria and form large aggregates. The images of bacteria solution interacted with different amounts of particles in Fig. S4 exhibited that particles/bacteria aggregation could even lead to spontaneous sedimentation. These aggregation and sedimentation phenomena could further increase the simplicity of separation operation and the removal efficiency of bacteria.[61]

In synthetic biology-related applications, the separation of large bacterial populations is often required, whereas in water treatment, food processing, disease diagnosis, and therapeutic applications, the bacterial concentrations in the relevant media are typically low.[9,62] To simulate various application scenarios, these PEI modified porous magnets were applied to separate different concentrations of bacteria. High concentration bacteria separation in Fig. 3(b–d) was designed to explore the adsorption capacity of each kind of PEI modified porous magnet for industrial applications.[63] The results showed that as the bacterial load increased, the adsorption capacity of the PEI-modified porous magnets initially increased and then decreased. For small molecules or ions, adsorption capacity generally rises with higher adsorbate concentrations due to enhanced mass transport.[28,64] However, for bacterial removal, all five particle sizes exhibited maximum adsorption capacity at an intermediate bacteria-to-particle ratio. This behavior likely arises because bacterial removal involves not only simple adsorption but also particle–bacteria flocculation, as suggested by Fig. 4 and Fig. S4. The initial increase in adsorption capacity reflects more complete utilization of the available binding sites on the PEI-modified porous magnets. At very high bacterial loads, however, excessive aggregation may be inhibited, reducing adsorption efficiency.[61] These observations indicate the existence of an optimal bacteria-to-particle ratio, which is important for maximizing the practical use of magnetic adsorbents. Additionally, with increasing bacterial amounts, the overall removal efficiency gradually decreased, highlighting a trade-off that should be considered depending on the specific application.[63]

The adsorption capacity of PEI modified porous magnets increased with the decrease of particle diameter, as shown in Fig. 3(b) and (d). The highest adsorption capacity of PPM_420 nm, PPM_360 nm, PPM_210 nm, and PPM_90 nm was 0.8×10^9, 1.1×10^9, 1.3×10^9, 2.5×10^9 CFU mg^{-1}, respectively. Especially, the smallest PPM_50 nm could achieve an extraordinary adsorption capacity as high as 18.8×10^9 CFU mg^{-1}, which exceeded all reported magnetic materials.[65,66] This positive correlation between adsorption capacity and decreasing particle size can be attributed to the larger specific surface area of smaller particles, which enhances interactions with bacteria. These results indicate that magnetic adsorbents with smaller particle diameters are particularly advantageous when high adsorption capacity is required. The findings from high-concentration bacterial separations offer valuable guidance for applications in synthetic biology.[63]

Considering environmental and biomedical applications, low-concentration bacterial separations were also investigated, with a focus on removal thoroughness (Fig. 3e and f).[67] After treatment with PEI-modified porous magnets, larger particles (PPM_420 nm and PPM_360 nm) achieved near-complete bacterial removal, approaching 100% efficiency, which is highly desirable for many practical applications.[68] In contrast, smaller particles (PPM_210 nm and PPM_90 nm), while exhibiting higher adsorption capacities at high bacterial concentrations, left residual bacteria at low concentrations (Fig. 3e). This behavior likely reflects the importance of an optimal bacteria-to-particle ratio, which promotes aggregation and rapid separation.[28] At low bacterial concentrations, although some magnetic particles can still attach to bacteria, the separation process relies primarily on the magnetic gradient force acting

on the particles, which may be insufficient to drive bacterial motion.[8] The superior performance of larger particles in these conditions can be attributed to their higher magnetic moments, which enable efficient magnetically driven separation rather than depending on aggregation. Moreover, the smallest PPM_50 nm was almost unusable in low bacteria separation and following adsorption kinetics exploration as they were extremely hard to separate without sufficient contact with bacteria to cancel out their electropositivity and induce aggregation. They would keep stable dispersion in supernatant (as shown in Fig. S4) due to their electrostatic repulsion and Brownian motion, which could potentially lead to residual contamination or toxicity issues.

To investigate bacterial separation kinetics, the adsorption capacities of PEI-modified porous magnets of different diameters were monitored as a function of reaction time (Fig. 3(g)). All particle sizes reached over 95% of their saturation adsorption capacity within 10 minutes, demonstrating rapid bacterial removal. This fast adsorption is attributed to the strong electrostatic interactions between the PEI coating and the negatively charged bacterial surfaces. In addition, with the decrease of particle diameter, the separation rate of porous magnets increased. Particles with large diameters (PPM_420 nm and PPM_360 nm) only led to a small amount of bacteria separation in the first 3 min, whereas particles with smaller diameters (PPM_210 nm and 90 nm) could achieve over 75% of maximum adsorption capacities.

Compared with many functionalized materials that could only bind with specific bacteria, the strong electropositivity of PEI modified porous magnets could enable the effective capture of both Gram-negative and Gram-positive pathogens.[54] Besides *E. coli* as the model of Gram-negative bacteria, we also explored the separation capacity of our PEI modified porous magnets for Gram-positive pathogens with *S. aureus* as the model, as shown in Fig. 5. High concentration *S. aureus* bacteria separation in Fig. 5(b–d) also showed that with the increase of bacteria content, the adsorption capacity of PEI modified porous magnets tended to increase then decrease and the removal efficiency kept decreasing. This trend mirrors the observations for *E. coli*, consistent with the electrostatic nature of particle–bacteria interactions. The STEM images of *S. aureus* interacting with PEI modified porous magnets in Fig. 5(e–i) also indicated they mediated the bridging and aggregation of bacteria. In addition, the adsorption capacity of each PEI modified porous magnet for *S. aureus* was 2.6×10^9, 3.3×10^9, 3.9×10^9, 5.9×10^9, and 28.9×10^9 CFU mg^{-1},

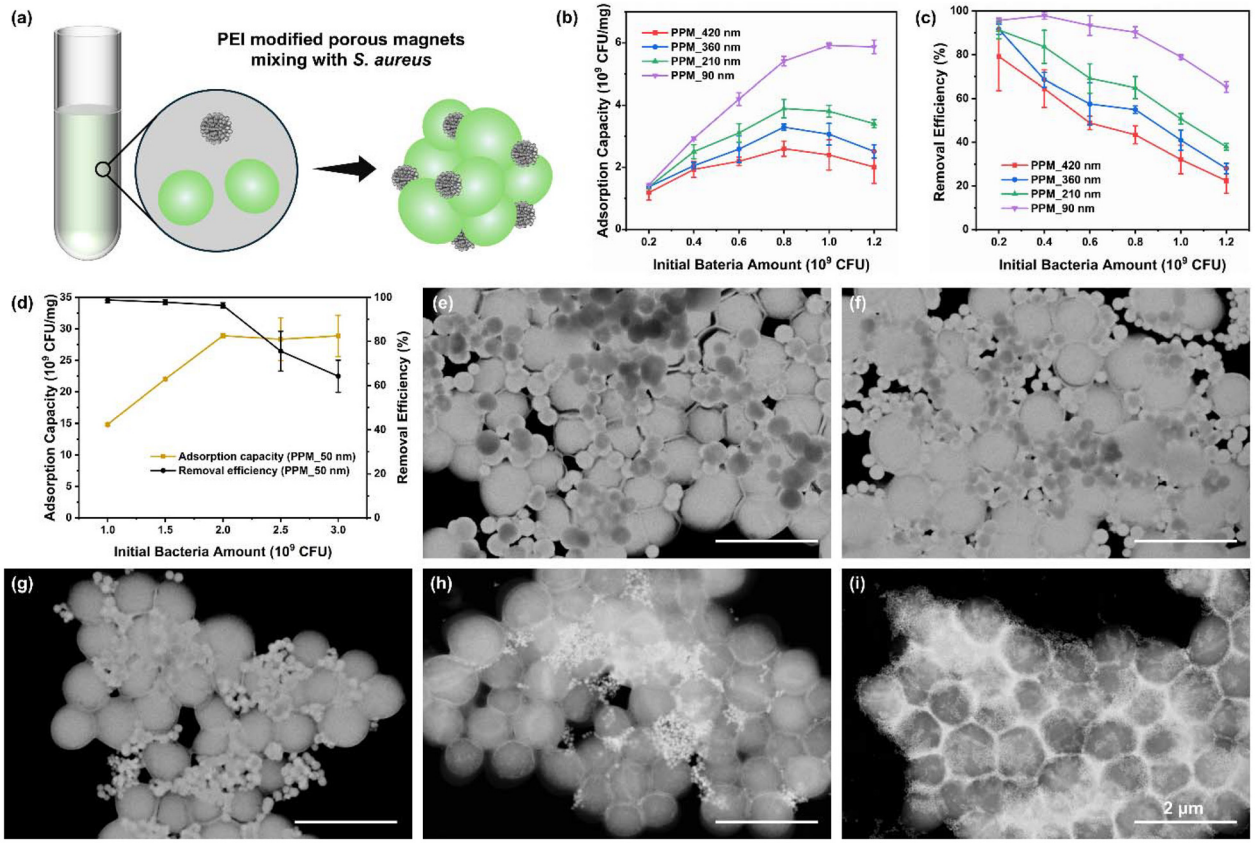

Fig. 5 Magnetic separation of *S. aureus* with PEI modified porous magnets. Scheme of interaction between *S. aureus* and PEI modified porous magnets (a). The adsorption capacity (b) and removal efficiency (c) of PPM_420 nm, PPM_360 nm, PPM_210 nm, PPM_90 nm with different initial bacteria amounts. The adsorption capacity and removal efficiency of PPM_50 nm with different initial bacteria amounts (d). The STEM images of *S. aureus* interacting with PPM_420 nm (e), PPM_360 nm (f), PPM_210 nm (g), PPM_90 nm (h), and PPM_50 nm (i).

respectively. The size effect, *e.g.*, smaller particles led to higher adsorption capacity, also matched well with previous observations.

4. Conclusion

We systematically investigated the influence of particle size on magnetic bacterial removal. A series of PEI-modified porous magnetic particles with tunable sizes (~50–420 nm) were synthesized to achieve efficient bacterial separation and systematically investigate size-dependent effects. These magnetic adsorbents induced extensive bacterial aggregation, including spontaneous sedimentation, and achieved high removal efficiencies for both Gram-negative *Escherichia coli* and Gram-positive *Staphylococcus aureus*. Adsorption capacity increased with decreasing particle size, and smaller particles exhibited faster adsorption kinetics. However, the smallest particles (50 nm) were difficult to recover from aqueous media without sufficient bacterial interaction, potentially leading to secondary contamination. In contrast, larger particles combined easy recovery with high removal efficiency, particularly at low bacterial concentrations. These results highlight the importance of particle size in designing effective magnetic adsorbents and provide practical guidance for applications in environmental remediation, biomedical treatment, and industrial bacterial separation.

Author contributions

J. C.: conceptualization, investigation, methodology, validation, visualization, formal analysis, data curation, writing – original draft; A. C.: conceptualization, investigation, methodology, validation, formal analysis, data curation, writing – review & editing; I. K.: investigation, methodology, formal analysis, writing – review & editing; Q. Z.: investigation, methodology, validation, formal analysis, data curation, supervision, project administration, writing – review & editing; V. C.: conceptualization, methodology, formal analysis, data curation, supervision, resources, project administration, writing – review & editing.

Conflicts of interest

The authors declare no conflict of interest.

Data availability

The data supporting this article have been included as part of the supplementary information (SI). Supplementary information is available. See DOI: https://doi.org/10.1039/d5nr03699b.

Acknowledgements

This work was supported by the National Science Foundation (ENG-2135687), Environmental Protection Agency (DV-84001801-0), and the National Institute of Health (R01EY030569). We sincerely thank Prof. Anita Shukla from Brown University for her help in providing *S. aureus* bacteria and FTIR detection. We also truly appreciate Prof. Kemp Plumb from Brown University for his help with VSM detection.

References

1 A. E. Mather, M. W. Gilmour, S. W. J. Reid and N. P. French, Foodborne Bacterial Pathogens: Genome-Based Approaches for Enduring and Emerging Threats in a Complex and Changing World, *Nat. Rev. Microbiol.*, 2024, 1–13, DOI: 10.1038/s41579-024-01051-z.
2 G. Hwang, A. J. Paula, E. E. Hunter, Y. Liu, A. Babeer, B. Karabucak, K. Stebe, V. Kumar, E. Steager and H. Koo, Catalytic Antimicrobial Robots for Biofilm Eradication, *Sci. Robot*, 2019, **4**(29), eaaw2388, DOI: 10.1126/scirobotics.aaw2388.
3 W. P. J. Smith, B. R. Wucher, C. D. Nadell and K. R. Foster, Bacterial Defences: Mechanisms, Evolution and Antimicrobial Resistance, *Nat. Rev. Microbiol.*, 2023, **21**(8), 519–534, DOI: 10.1038/s41579-023-00877-3.
4 C. C. Mayorga-Martinez, L. Zhang and M. Pumera, Chemical Multiscale Robotics for Bacterial Biofilm Treatment, *Chem. Soc. Rev.*, 2024, **53**(5), 2284–2299, DOI: 10.1039/D3CS00564J.
5 J. Chen, S. M. Andler, J. M. Goddard, S. R. Nugen and V. M. Rotello, Integrating Recognition Elements with Nanomaterials for Bacteria Sensing, *Chem. Soc. Rev.*, 2017, **46**(5), 1272–1283, DOI: 10.1039/c6cs00313c.
6 X.-L. Gao, M.-F. Shao, Y.-S. Xu, Y. Luo, K. Zhang, F. Ouyang and J. Li, Non-Selective Separation of Bacterial Cells with Magnetic Nanoparticles Facilitated by Varying Surface Charge, *Front. Microbiol.*, 2016, **7**, 1891, DOI: 10.3389/fmicb.2016.01891.
7 F.-Y. Kuo, W.-L. Lin and Y.-C. Chen, Affinity Capture Using Peptide-Functionalized Magnetic Nanoparticles to Target *Staphylococcus Aureus*, *Nanoscale*, 2016, **8**(17), 9217–9225, DOI: 10.1039/c6nr00368k.
8 S. S. Leong, S. P. Yeap and J. Lim, Working Principle and Application of Magnetic Separation for Biomedical Diagnostic at High- and Low-Field Gradients, *Interface Focus*, 2016, **6**(6), 20160048, DOI: 10.1098/rsfs.2016.0048.
9 E. M. Jones, J. P. Marken and P. A. Silver, Synthetic Microbiology in Sustainability Applications, *Nat. Rev. Microbiol.*, 2024, **22**(6), 345–359, DOI: 10.1038/s41579-023-01007-9.
10 J. J. Hug, D. Krug and R. Müller, Bacteria as Genetically Programmable Producers of Bioactive Natural Products, *Nat. Rev. Chem.*, 2020, **4**(4), 172–193, DOI: 10.1038/s41570-020-0176-1.

11 S. M. Brooks and H. S. Alper, Applications, Challenges, and Needs for Employing Synthetic Biology beyond the Lab, *Nat. Commun.*, 2021, **12**(1), 1390, DOI: 10.1038/s41467-021-21740-0.
12 K. A. Stevens and L.-A. Jaykus, Bacterial Separation and Concentration from Complex Sample Matrices: A Review, *Crit. Rev. Microbiol.*, 2004, **30**(1), 7–24, DOI: 10.1080/10408410490266410.
13 M. Iranmanesh and J. Hulliger, Magnetic Separation: Its Application in Mining, Waste Purification, Medicine, Biochemistry and Chemistry, *Chem. Soc. Rev.*, 2017, **46**(19), 5925–5934, DOI: 10.1039/C7CS00230K.
14 X. Bai, A. Shen and J. Hu, A Sensitive SERS-Based Sandwich Immunoassay Platform for Simultaneous Multiple Detection of Foodborne Pathogens without Interference, *Anal. Methods*, 2020, **12**(40), 4885–4891, DOI: 10.1039/d0ay01541e.
15 C. Li, Z. Li, Y. Gan, F. Jiang, H. Zhao, J. Tan, Y. Y. Yang, P. Yuan and X. Ding, Selective Capture, Separation, and Photothermal Inactivation of Methicillin-Resistant Staphylococcus Aureus (MRSA) Using Functional Magnetic Nanoparticles, *ACS Appl. Mater. Interfaces*, 2022, **14**(18), 20566–20575, DOI: 10.1021/acsami.1c24102.
16 J. Chen, B. Duncan, Z. Wang, L.-S. Wang, V. M. Rotello and S. R. Nugen, Bacteriophage-Based Nanoprobes for Rapid Bacteria Separation, *Nanoscale*, 2015, **7**(39), 16230–16236, DOI: 10.1039/c5nr03779d.
17 S. M. You, K. Luo, J. Y. Jung, K. B. Jeong, E. S. Lee, M. H. Oh and Y. R. Kim, Gold Nanoparticle-Coated Starch Magnetic Beads for the Separation, Concentration, and SERS-Based Detection of E. Coli O157:H7, *ACS Appl. Mater. Interfaces*, 2020, **12**(16), 18292–18300, DOI: 10.1021/acsami.0c00418.
18 E. Dester and E. Alocilja, Current Methods for Extraction and Concentration of Foodborne Bacteria with Glycan-Coated Magnetic Nanoparticles: A Review, *Biosensors*, 2022, **12**(2), 112, DOI: 10.3390/bios12020112.
19 Z. Wei, Z. Zhou, M. Yang, C. Lin, Z. Zhao, D. Huang, Z. Chen and J. Gao, Multifunctional Ag@Fe2O3 Yolk–Shell Nanoparticles for Simultaneous Capture, Kill, and Removal of Pathogen, *J. Mater. Chem.*, 2011, **21**(41), 16344–16348, DOI: 10.1039/c1jm13691g.
20 Q. Sun, G. Zhao and W. Dou, Blue Silica Nanoparticle-Based Colorimetric Immunoassay for Detection of *Salmonella Pullorum*, *Anal. Methods*, 2015, **7**(20), 8647–8654, DOI: 10.1039/c5ay02073e.
21 T. Banerjee, S. Sulthana, T. Shelby, B. Heckert, J. Jewell, K. Woody, V. Karimnia, J. McAfee and S. Santra, Multiparametric Magneto-Fluorescent Nanosensors for the Ultrasensitive Detection of *Escherichia Coli*, O157:H7, *ACS Infect. Dis.*, 2016, **2**(10), 667–673, DOI: 10.1021/acsinfecdis.6b00108.
22 H. Kearns, R. Goodacre, L. E. Jamieson, D. Graham and K. Faulds, SERS Detection of Multiple Antimicrobial-Resistant Pathogens Using Nanosensors, *Anal. Chem.*, 2017, **89**(23), 12666–12673, DOI: 10.1021/acs.analchem.7b02653.
23 S. Ma, S. Zhan, Y. Jia and Q. Zhou, Highly Efficient Antibacterial and Pb(II) Removal Effects of Ag-CoFe2O4-GO Nanocomposite, *ACS Appl. Mater. Interfaces*, 2015, **7**(19), 10576–10586, DOI: 10.1021/acsami.5b02209.
24 C. Xu, O. U. Akakuru, J. Zheng and A. Wu, Applications of Iron Oxide-Based Magnetic Nanoparticles in the Diagnosis and Treatment of Bacterial Infections, *Front. Bioeng. Biotechnol.*, 2019, **7**, 141, DOI: 10.3389/fbioe.2019.00141.
25 N. Bohmer, N. Demarmels, E. Tsolaki, L. Gerken, K. Keevend, S. Bertazzo, M. Lattuada and I. K. Herrmann, Removal of Cells from Body Fluids by Magnetic Separation in Batch and Continuous Mode: Influence of Bead Size, Concentration, and Contact Time, *ACS Appl. Mater. Interfaces*, 2017, **9**(35), 29571–29579, DOI: 10.1021/acsami.7b10140.
26 S. S. Leong, Z. Ahmad, J. Camacho, J. Faraudo and J. Lim, Kinetics of Low Field Gradient Magnetophoresis in the Presence of Magnetically Induced Convection, *J. Phys. Chem. C*, 2017, **121**(9), 5389–5407, DOI: 10.1021/acs.jpcc.6b13090.
27 K. Witte, K. Müller, C. Grüttner, F. Westphal and C. Johansson, Particle Size- and Concentration-Dependent Separation of Magnetic Nanoparticles, *J. Magn. Magn. Mater.*, 2017, **427**, 320–324, DOI: 10.1016/j.jmmm.2016.11.006.
28 J. Chen, Q. Cao and X. Han, Smart Water-Based Ferrofluid with Stable State Transition Property: Preparation and Its Application in Anionic Dye Removal, *J. Cleaner Prod.*, 2021, **287**, 125003, DOI: 10.1016/j.jclepro.2020.125003.
29 H. Lee, D. Hong, H. Cho, J. Y. Kim, J. H. Park, S. H. Lee, H. M. Kim, R. F. Fakhrullin and I. S. Choi, Turning Diamagnetic Microbes into Multinary Micro-Magnets: Magnetophoresis and Spatio-Temporal Manipulation of Individual Living Cells, *Sci. Rep.*, 2016, **6**, 38517, DOI: 10.1038/srep38517.
30 M. Hejazian, W. Li and N. Nam-Trung, Lab on a Chip for Continuous-Flow Magnetic Cell Separation, *Lab Chip*, 2015, **15**(4), 959–970, DOI: 10.1039/c4lc01422g.
31 Y. Liu, Y. Li, X.-M. Li and T. He, Kinetics of (3-Aminopropyl)Triethoxylsilane (APTES) Silanization of Superparamagnetic Iron Oxide Nanoparticles, *Langmuir*, 2013, **29**(49), 15275–15282, DOI: 10.1021/la403269u.
32 C. Lastoskie, K. E. Gubbins and N. Quirke, Pore Size Distribution Analysis of Microporous Carbons: A Density Functional Theory Approach, *J. Phys. Chem.*, 1993, **97**, 4786–4796, DOI: 10.1021/j100120a035.
33 Z. Lu and Y. Yin, Colloidal Nanoparticle Clusters: Functional Materials by Design, *Chem. Soc. Rev.*, 2012, **41**(21), 6874–6887, DOI: 10.1039/c2cs35197h.
34 J. Ge, Y. Hu, M. Biasini, W. P. Beyermann and Y. Yin, Superparamagnetic Magnetite Colloidal Nanocrystal Clusters, *Angew. Chem., Int. Ed.*, 2007, **46**(23), 4342–4345, DOI: 10.1002/anie.200700197.
35 Z. Xiao, L. Zhang, V. L. Colvin, Q. Zhang and G. Bao, Synthesis and Application of Magnetic Nanocrystal

Clusters, *Ind. Eng. Chem. Res.*, 2022, **61**(22), 7613–7625, DOI: 10.1021/acs.iecr.1c04879.

36 T. Wang, L. Zhang, H. Wang, W. Yang, Y. Fu, W. Zhou, W. Yu, K. Xiang, Z. Su, S. Dai and L. Chai, Controllable Synthesis of Hierarchical Porous Fe3O4 Particles Mediated by Poly(Diallyldimethylammonium Chloride) and Their Application in Arsenic Removal, *ACS Appl. Mater. Interfaces*, 2013, **5**(23), 12449–12459, DOI: 10.1021/am403533v.

37 Z. Xiao, Q. Zhang, X. Guo, J. Villanova, Y. Hu, I. Külaots, D. Garcia-Rojas, W. Guo and V. L. Colvin, Libraries of Uniform Magnetic Multicore Nanoparticles with Tunable Dimensions for Biomedical and Photonic Applications, *ACS Appl. Mater. Interfaces*, 2020, **12**(37), 41932–41941, DOI: 10.1021/acsami.0c09778.

38 S. Effman, S. Avidan, Z. Xiao and V. Colvin, Stable Aqueous Suspensions of Manganese Ferrite Clusters with Tunable Nanoscale Dimension and Composition, *J. Visualized Exp.*, 2022, (180), e63140, DOI: 10.3791/63140.

39 G. Tong, Y. Liu, T. Wu, C. Tong and F. Du, H_2O-Steered Size/Phase Evolution and Magnetic Properties of Large-Scale, Monodisperse FexOy Nanomaterials, *J. Mater. Chem. C*, 2015, **3**(21), 5506–5515, DOI: 10.1039/c5tc00347d.

40 Z. Huang, K. Wu, Q.-H. Yu, Y.-Y. Wang, J. Xing and T.-L. Xia, Facile Synthesis of Size Tunable Fe3O4 Nanoparticles in Bisolvent System, *Chem. Phys. Lett.*, 2016, **664**, 219–225, DOI: 10.1016/j.cplett.2016.10.036.

41 A. Bunge, A. S. Porav, G. Borodi, T. Radu, A. Pirnau, C. Berghian-Grosan and R. Turcu, Correlation between Synthesis Parameters and Properties of Magnetite Clusters Prepared by Solvothermal Polyol Method, *J. Mater. Sci.*, 2019, **54**(4), 2853–2875, DOI: 10.1007/s10853-018-3030-9.

42 C. Cheng, Y. Wen, X. Xu and H. Gu, Tunable Synthesis of Carboxyl-Functionalized Magnetite Nanocrystal Clusters with Uniform Size, *J. Mater. Chem.*, 2009, **19**(46), 8782–8788, DOI: 10.1039/b910832g.

43 A. H. Oh, H.-Y. Park, Y.-G. Jung, S.-C. Choi and G. S. An, Synthesis of Fe3O4 Nanoparticles of Various Size via the Polyol Method, *Ceram. Int.*, 2020, **46**(8, Part A), 10723–10728, DOI: 10.1016/j.ceramint.2020.01.080.

44 Y. Liu, W. Luo, Q. Fan, H. Ma, Y. Yin, Y. Long and J. Guan, Polyphenol-Mediated Synthesis of Superparamagnetic Magnetite Nanoclusters for Highly Stable Magnetically Responsive Photonic Crystals, *Adv. Funct. Mater.*, 2023, **33**, 2303470, DOI: 10.1002/adfm.202303470.

45 L. Zhang, Q. Zhang, D. T. Hinojosa, K. Jiang, Q.-K. Pham, Z. Xiao, V. L. Colvin and G. Bao, Multifunctional Magnetic Nanoclusters Can Induce Immunogenic Cell Death and Suppress Tumor Recurrence and Metastasis, *ACS Nano*, 2022, **16**(11), 18538–18554, DOI: 10.1021/acsnano.2c06776.

46 C. Amador and L. Martin de Juan, Chapter 19 - Strategies for Structured Particulate Systems Design, in *Computer Aided Chemical Engineering*, ed. M. Martín, M. R. Eden and N. G. Chemmangattuvalappil, Tools For Chemical Product Design, Elsevier, 2016, vol. 39, pp. 509–579. DOI: 10.1016/B978-0-444-63683-6.00019-8.

47 L. Xiong, J. Bi, Y. Tang and S.-Z. Qiao, Magnetic Core-Shell Silica Nanoparticles with Large Radial Mesopores for siRNA Delivery, *Small*, 2016, **12**(34), 4735–4742, DOI: 10.1002/smll.201600531.

48 A. Heuer-Jungemann, N. Feliu, I. Bakaimi, M. Hamaly, A. Alkilany, I. Chakraborty, A. Masood, M. F. Casula, A. Kostopoulou, E. Oh, K. Susumu, M. H. Stewart, I. L. Medintz, E. Stratakis, W. J. Parak and A. G. Kanaras, The Role of Ligands in the Chemical Synthesis and Applications of Inorganic Nanoparticles, *Chem. Rev.*, 2019, **119**(8), 4819–4880, DOI: 10.1021/acs.chemrev.8b00733.

49 I. Migneault, C. Dartiguenave, M. J. Bertrand and K. C. Waldron, Glutaraldehyde: Behavior in Aqueous Solution, Reaction with Proteins, and Application to Enzyme Crosslinking, *BioTechniques*, 2004, **37**(5), 790–802, DOI: 10.2144/04375RV01.

50 A. Rajan, M. Sharma and N. K. Sahu, Assessing Magnetic and Inductive Thermal Properties of Various Surfactants Functionalised Fe3O4 Nanoparticles for Hyperthermia, *Sci. Rep.*, 2020, **10**, 15045, DOI: 10.1038/s41598-020-71703-6.

51 J. Li, S. Yuan, J. Zhu and B. Van der Bruggen, High-Flux, Antibacterial Composite Membranes via Polydopamine-Assisted PEI-TiO2/Ag Modification for Dye Removal, *Chem. Eng. J.*, 2019, **373**, 275–284, DOI: 10.1016/j.cej.2019.05.048.

52 Y. Lu, L. Fan, L.-Y. Yang, F. Huang and X. Ouyang, PEI-Modified Core-Shell/Bead-like Amino Silica Enhanced Poly (Vinyl Alcohol)/Chitosan for Diclofenac Sodium Efficient Adsorption, *Carbohydr. Polym.*, 2020, **229**, 115459, DOI: 10.1016/j.carbpol.2019.115459.

53 S. M. Pormazar, M. H. Ehrampoush, M. T. Ghaneian, M. Khoobi, P. Talebi and A. Dalvand, Application of Amine-Functioned Fe3O4 Nanoparticles with HPEI for Effective Humic Acid Removal from Aqueous Solution: Modeling and Optimization, *Korean J. Chem. Eng.*, 2020, **37**(1), 93–104, DOI: 10.1007/s11814-019-0411-y.

54 Y. Jin, F. Liu, C. Shan, M. Tong and Y. Hou, Efficient Bacterial Capture with Amino Acid Modified Magnetic Nanoparticles, *Water Res.*, 2014, **50**, 124–134, DOI: 10.1016/j.watres.2013.11.045.

55 Y. Zhang, B. Du, Y. Wu, Z. Liu, J. Wang, J. Xu, Z. Tong, X. Mu and B. Liu, Fe(3)O(4)@PDA@PEI Core-Shell Microspheres as a Novel Magnetic Sorbent for the Rapid and Broad-Spectrum Separation of Bacteria in Liquid Phase, *Materials*, 2022, **15**(6), 2039, DOI: 10.3390/ma15062039.

56 A. Valverde, A. Cabrera-Codony, M. Calvo-Schwarzwalder and T. G. Myers, Investigating the Impact of Adsorbent Particle Size on Column Adsorption Kinetics through a Mathematical Model, *Int. J. Heat Mass Transfer*, 2024, **218**, 124724, DOI: 10.1016/j.ijheatmasstransfer.2023.124724.

57 K. H. Jacobson, I. L. Gunsolus, T. R. Kuech, J. M. Troiano, E. S. Melby, S. E. Lohse, D. Hu, W. B. Chrisler, C. J. Murphy, G. Orr, F. M. Geiger, C. L. Haynes and J. A. Pedersen, Lipopolysaccharide Density and Structure Govern the Extent and Distance of Nanoparticle Interaction with Actual and Model Bacterial Outer Membranes,

Environ. Sci. Technol., 2015, **49**(17), 10642–10650, DOI: 10.1021/acs.est.5b01841.

58 M. Gross, S. E. Cramton, F. Götz and A. Peschel, Key Role of Teichoic Acid Net Charge in Staphylococcus Aureus Colonization of Artificial Surfaces, *Infect. Immun.*, 2001, **69**(5), 3423–3426, DOI: 10.1128/IAI.69.5.3423-3426.2001.

59 W. C. McGregor and R. K. Finn, Factors Affecting the Flocculation of Bacteria by Chemical Additives, *Biotechnol. Bioeng.*, 1969, **11**(2), 127–138, DOI: 10.1002/bit.260110203.

60 B. Oyegbile, P. Ay and S. Narra, Flocculation Kinetics and Hydrodynamic Interactions in Natural and Engineered Flow Systems: A Review, *Environ. Eng. Res.*, 2016, **21**(1), 1–14, DOI: 10.4491/eer.2015.086.

61 H. Li, S. Wu, C. Du, Y. Zhong and C. Yang, Preparation, Performances, and Mechanisms of Microbial Flocculants for Wastewater Treatment, *Int. J. Environ. Res. Public Health*, 2020, **17**(4), 1360, DOI: 10.3390/ijerph17041360.

62 Z. Niu, C. Chen, Z. Yin, X. Zhang, J. Sun and H. Shi, Mechanism Insight into the Fe3O4/Biochar/BiOBr S–Scheme Heterostructure with Improved Photocatalytic Degradation Performance for Pharmaceutical Wastewater, *Colloids Surf., A*, 2026, **728**, 138518, DOI: 10.1016/j.colsurfa.2025.138518.

63 J. E. Petch, P. Gurnani, G. Yilmaz, F. Mastrotto, C. Alexander, S. Heeb, M. Camara and G. Mantovani, Combining Inducible Lectin Expression and Magnetic Glyconanoparticles for the Selective Isolation of Bacteria from Mixed Populations, *ACS Appl. Mater. Interfaces*, 2021, **13**(16), 19230–19243, DOI: 10.1021/acsami.1c00907.

64 J. Chen, L. Xia and Q. Cao, Water-Based Ferrofluid with Tunable Stability and Its Significance in Nuclear Wastewater Treatment, *J. Hazard. Mater.*, 2022, **434**, 128893, DOI: 10.1016/j.jhazmat.2022.128893.

65 K. Luo, K.-B. Jeong, S.-M. You, D.-H. Lee, J.-Y. Jung and Y.-R. Kim, Surface-Engineered Starch Magnetic Microparticles for Highly Effective Separation of a Broad Range of Bacteria, *ACS Sustainable Chem. Eng.*, 2018, **6**(10), 13524–13531, DOI: 10.1021/acssuschemeng.8b03611.

66 Z. Chang, Z. Wang, M. Lu, M. Li, L. Li, Y. Zhang, D. Shao and W. Dong, Magnetic Janus Nanorods for Efficient Capture, Separation and Elimination of Bacteria, *RSC Adv.*, 2017, **7**(6), 3550–3553, DOI: 10.1039/c6ra27296g.

67 W. G. Pitt, M. Alizadeh, G. A. Husseini, D. S. McClellan, C. M. Buchanan, C. G. Bledsoe, R. A. Robison, R. Blanco, B. L. Roeder, M. Melville and A. K. Hunter, Rapid Separation of Bacteria from Blood—Review and Outlook, *Biotechnol. Prog.*, 2016, **32**(4), 823–839, DOI: 10.1002/btpr.2299.

68 J. Du, K. Liu, J. Liu, D. Zhao and Y. Bai, Development of a Novel Lateral Flow Immunoassay Based on Fe_3O_4@MIL-100 (Fe) for Visual Detection of *Listeria Monocytogenes*, *J. Food Meas. Charact.*, 2023, **17**(4), 3482–3492, DOI: 10.1007/s11694-023-01900-0.